Nanotechnology

DOI: 10.1002/anie.201408638

Inkjet Printing and Instant Chemical Transformation of a $CH_3NH_3PbI_3$/Nanocarbon Electrode and Interface for Planar Perovskite Solar Cells**

*Zhanhua Wei, Haining Chen, Keyou Yan, and Shihe Yang**

Abstract: *A planar perovskite solar cell that incorporates a nanocarbon hole-extraction layer is demonstrated for the first time by an inkjet printing technique with a precisely controlled pattern and interface. By designing the carbon plus CH_3NH_3I ink to transform PbI_2 in situ to $CH_3NH_3PbI_3$, an interpenetrating seamless interface between the $CH_3NH_3PbI_3$ active layer and the carbon hole-extraction electrode was instantly constructed, with a markedly reduced charge recombination compared to that with the carbon ink alone. As a result, a considerably higher power conversion efficiency up to 11.60% was delivered by the corresponding solar cell. This method provides a major step towards the fabrication of low-cost, large-scale, metal-electrode-free but still highly efficient perovskite solar cells.*

In the last five years, hybrid organic–inorganic perovskite solar cells have experienced an explosive development, with a power conversion efficiency (PCE) rising from the initial 3% to a certified 17.9%, and most recently, up to 19.3%.[1–11] What have transpired are the ideal photovoltaic properties of the perovskite materials ($CH_3NH_3PbI_3$ and $CH_3NH_3PbI_{3-x}Cl_x$), such as appropriate and tunable direct band gap, high absorption coefficient, highly mobile electron and holes,[12] excellent (balanced) carrier transport diffusion length (100 to 1000 nm),[13] and apparent tolerance of defects. Furthermore, the perovskite materials are solution-processable and low-cost. With an in-depth understanding of their working mechanism and judicious design and controllable fabrication, over 20% PCE perovskite solar cells are expected in the near future.

A typical perovskite solar cell consists of TiO_2 (mesoporous or compact), $CH_3NH_3PbI_3$, hole transport material (HTM) and noble metal counter electrode.[14,15] Discouragingly, the conventional organic hole transporter materials (such as spiro-OMeTAD) are expensive and unstable.[16,17] The noble metal electrode is also costly and requires demanding vacuum thermal evaporation deposition. To solve these problems, some inorganic hole-transport materials[18,19] and hole-extraction materials[20–26] have been developed for perovskite solar cells. Among those materials, carbon materials themselves stand out because of the suitable Fermi level, earth abundance, low cost, and superior environmental stability.[27–29] In one type of carbon-based perovskite solar cells, a mesoporous TiO_2 layer, a ZrO_2 insulating layer, and a carbon electrode are sequentially deposited, followed by infiltration of a perovskite precursor solution, which requires perfect pore filling to ensure high performance.[25,27,28] In previous work, we demonstrated a new and simplified configuration for the carbon-based perovskite solar cells, which embodies the two-step formation of the perovskite layer and the eliminating of the ZrO_2 insulating layer.[30] The beauty of the design is that a pre-deposited PbI_2 layer plays the role of the aforementioned ZrO_2 layer in separation the TiO_2 and the carbon layer, but is transformed to the perovskite layer at a later stage. The energy conversion efficiency of such carbon based perovskite solar cells reached values as high as 11.06%.

The carbon-based perovskite solar cells appear to be quite compatible with the powerful printing technology, which would allow large-scale and low-cost production. However, the printable perovskite solar cells of this type have not been demonstrated until now, not to mention the chemical transformation and the interface development associated with the printing process. To tackle this problem, we have developed an inkjet printing technique, which permits instant formation of a conformable $CH_3NH_3PbI_3$/C bilayer with programmable control. Importantly, this ink printing technique enables a planar configuration, which is regarded as the configuration of choice for perovskite solar cells because of the potential benefits of large grain size and defect-free boundary, permitting long range balanced electron–hole diffusion.[6,31–37] Another salient innovation is the formulation of the C + CH_3NH_3I ink to simultaneously deposit the nanocarbon electrode, transform PbI_2 to $CH_3NH_3PbI_3$ in situ, and create an interpenetrating interface between $CH_3NH_3PbI_3$ and C electrode with minimal charge recombination. This inkjet printed carbon-based planar perovskite solar cell has registered a considerably high efficiency up to 11.60%.

Figure 1 illustrates the strategies we used to prepare TiO_2/$CH_3NH_3PbI_3$/C planar solar cells by inkjet printing technique. In step 1, a TiO_2 compact layer was deposited on a FTO glass by $TiCl_4$ treatment. Then, a PbI_2 thin film was deposited on the TiO_2 compact layer by multiple spin-coating runs (step 2). The conversion of PbI_2 into $CH_3NH_3PbI_3$ and the simultaneous deposition of a carbon hole-extraction layer were accomplished by two different strategies were applied. One

[*] Z. Wei,[+] Dr. H. Chen,[+] Dr. K. Yan, Prof. S. Yang
Department of Chemistry
William Mong Institute of Nano Science and Technology
The Hong Kong University of Science and Technology
Clear Water Bay, Kowloon, Hong Kong (China)
E-mail: chsyang@ust.hk

[+] These authors contributed equally to this work.

[**] This work was supported by the HK-RGC General Research Funds (GRE No. HKUST 606511, 605710).

Supporting information for this article is available on the WWW under http://dx.doi.org/10.1002/anie.201408638.

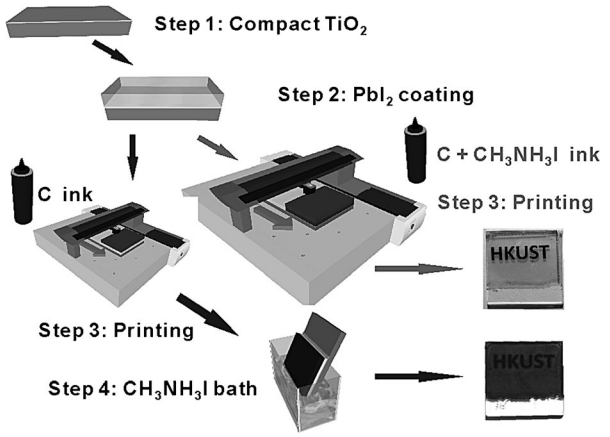

Figure 1. Fabrication process flow for the instant inkjet printing of the C/$CH_3NH_3PbI_3$ planar perovskite solar cells. For comparison, a different strategy was used to convert PbI_2 into $CH_3NH_3PbI_3$ using a separate step 3 and step 4 (see text for details).

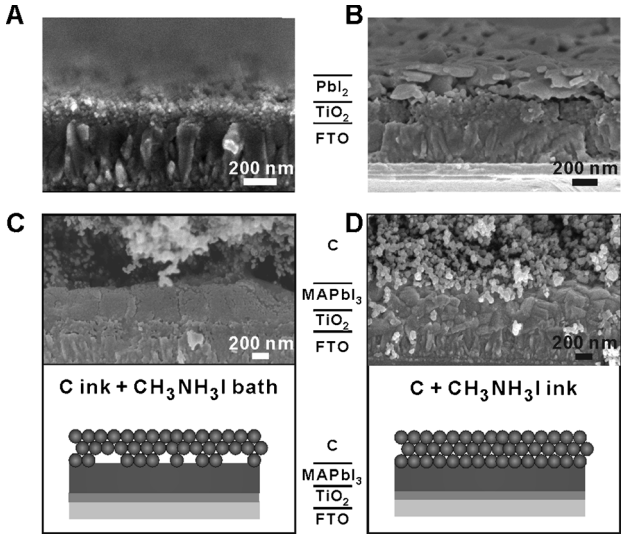

Figure 2. A) Cross-sectional SEM image of TiO_2 compact layer grown by $TiCl_4$ treatment. B) Cross-sectional SEM image of TiO_2/PbI_2 thin film prepared by multiple spin-coating. C), D) Cross-sectional SEM images and the corresponding diagrams of TiO_2/$CH_3NH_3PbI_3$/C solar cells prepared by the inkjet printing technique using the C ink (C) and the C + CH_3NH_3I ink (D).

strategy (black arrows) was to first print carbon black ink (carbon black dispersed in isopropanol solution) on the PbI_2 layer (step 3), followed by immersion into a CH_3NH_3I bath to obtain the final TiO_2/$CH_3NH_3PbI_3$/C planar solar cell (step 4). As for the second strategy (gray arrows), step 3 and step 4 in the first strategy were combined (namely, step 3 only here). To this end, a reactive ink was prepared by mixing carbon black and CH_3NH_3I in isopropanol together. Through the modified step 3, the PbI_2 layer can be converted into $CH_3NH_3PbI_3$ instantly, resulting in improved interfaces of TiO_2/$CH_3NH_3PbI_3$/C. It is worth pointing out that a heating process (1 hour) is needed for both strategies after carbon electrode printing (ca. 5 seconds).

Through inkjet printing, the carbon electrode could be precisely patterned in planar solar cells (the printer modification can be found in the Supporting Information, Figure S1). As shown in Figure 1, the carbon electrodes with "HKUST" patterns were successfully and precisely achieved. Moreover, it is clear that only the PbI_2 covered by the "HKUST" pattern was converted to $CH_3NH_3PbI_3$ for strategy 2, whereas all the PbI_2 was converted into $CH_3NH_3PbI_3$ for strategy 1, highlighting the patterning advantage of the combined ink of C + CH_3NH_3I. For a practical test, rectangle carbon electrodes were printed on the perovskite thin films. To the best of our knowledge, this is the first report of the programmable fabrication of perovskites solar cells, and this fast and controllable printing technique is a step forward for developing commercial perovskite solar cells.

To evaluate the interfacial connectivity of the TiO_2/$CH_3NH_3PbI_3$/C solar cells prepared by the two different inkjet printing strategies, we first turned to scanning electron microscopy (SEM). Basically, a successful planar perovskite solar cells requires a compact layer of TiO_2 or ZnO with a sufficient roughness to block holes and to support/ensure a mechanically robust perovskite layer.[1,3,36–39] In step 1, the TiO_2 layer was deposited on an FTO glass by $TiCl_4$ treatment. As shown in Figure 2 A, the as-prepared TiO_2 layer is indeed very compact and rough, with a thickness of about 150 nm. The X-ray diffraction pattern (Supporting Information, Figure S2) clearly reveals a rutile phase (JPCDS 011292) of the TiO_2 compact layer. In step 2, the PbI_2 thin film was prepared by the multiple spin-coating method. The concentration of the precursor solution and the spinning rate were carefully controlled to obtain a fully covered and well-connected PbI_2 thin film. As shown in Figure 2 B, a circa 300 nm thick PbI_2 thin film with a clear sheet structure covers well the TiO_2 compact layer. For step 3, two different inks were used. For preparing the C ink, carbon black (Supporting Information, Figure S3) was dispersed in isopropanol at a concentration of 15 mg mL^{-1}, while the preparation of the C + CH_3NH_3I ink was accomplished by adding CH_3NH_3I (10 mg mL^{-1}) into the above pristine C ink. Figure 2 C represents the cross-sectional SEM image of a TiO_2/$CH_3NH_3PbI_3$/C solar cell prepared by applying the C ink and the subsequent CH_3NH_3I bath. It is a clear layer by layer structure with a circa 350 nm thick $CH_3NH_3PbI_3$ thin film covered by a carbon layer. However, the contact between $CH_3NH_3PbI_3$ and C is not very intimate and some large pinholes are visible at the interface. By comparison, the SEM image of the TiO_2/$CH_3NH_3PbI_3$/C solar cell prepared by applying the C + CH_3NH_3I ink (Figure 2 D) presents a similar layer by layer structure but with a better-defined crystallinity in the $CH_3NH_3PbI_3$ thin film and more importantly, a better interface quality between the C and $CH_3NH_3PbI_3$ layers. The significantly improved C/$CH_3NH_3PbI_3$ interface with the C + CH_3NH_3I ink is presumably a result of the in situ chemical transformation and the carbon electrode deposition at the same time. More in-depth discussion about the successful fabrication of planar perovskite solar cell can be found in the Supporting Information, Figure S4. The improvement of the crystalline structure and the interface is pivotal to the superior photovoltaic performance, as will be shown below.

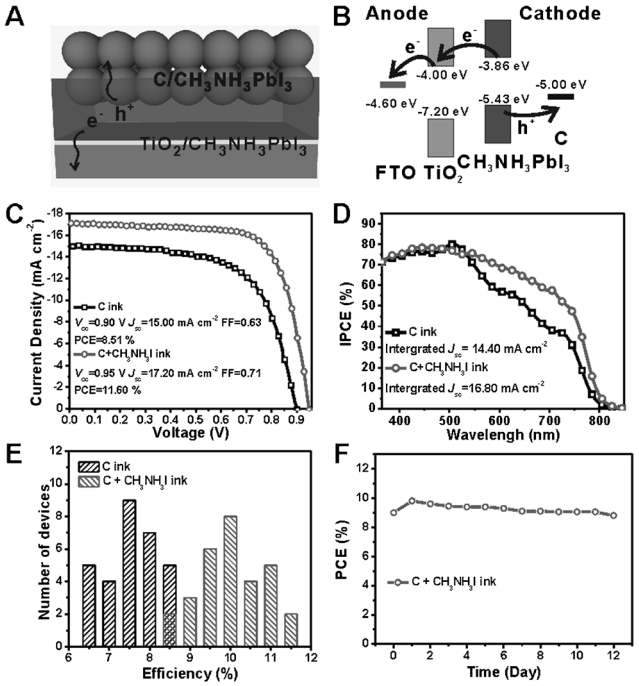

Figure 3. Photovoltaic performance of the $TiO_2/CH_3NH_3PbI_3$/C solar cells fabricated with different printing inks: A) The basic cell configuration, (B) energy level diagram, C) *J–V* curves, D) IPCE and E) PCE distribution profiles of solar cells based on the C ink and the $C+CH_3NH_3I$ ink. F) Long-term stability testing result for the $C+CH_3NH_3I$ ink devices. For this experiment, un-encapsulated devices were stored in ambient air (temperature: 25 °C, humidity: ca. 30 %) and tested every day.

The final structure of the $TiO_2/CH_3NH_3PbI_3$/C solar cells is indicated in Figure 3 A. The energy level diagram and charge transfer and transport processes in the solar cells are illustrated in Figure 3 B. When $CH_3NH_3PbI_3$ is excited by light illumination, electrons and holes are generated in the conduction band (CB) and value band (VB) of $CH_3NH_3PbI_3$, respectively. With the appropriate energy level alignments, electron injection happens at the $TiO_2/CH_3NH_3PbI_3$ interface from the CB (−3.86 eV) of $CH_3NH_3PbI_3$ to the CB of TiO_2 (−4.00 eV), and the final collection is carried out by the FTO glass. In parallel, the holes are extracted by C through the $C/CH_3NH_3PbI_3$ interface from the VB (−5.43 eV) of $CH_3NH_3PbI_3$ to C (Fermi level: −5.00 eV).

Figure 3 C shows the *J–V* curves of the two $TiO_2/CH_3NH_3PbI_3$/C solar cells. It can be seen that the solar cells prepared with the $C+CH_3NH_3I$ ink have an obviously higher performance than that prepared by the C ink. Specifically, the latter solar cells gives a V_{oc} of 0.90 V, J_{sc} of 15.00 mA cm^{-2}, FF of 0.63, and a PCE of 8.51 %, while the former presents a V_{oc} of 0.95 V, J_{sc} of 17.20 mA cm^{-2}, FF of 0.71, and a PCE of 11.60 %. To specify the ratio of extracted current to incident photons at a given wavelength, the incident photon-to-electron conversion efficiency (IPCE) spectra were recorded. As shown in Figure 3 D, the IPCE spectrum of the solar cells prepared by C ink gives a high value (larger than 70 %) before 550 nm but rapidly decreases above 550 nm and the cut off is at about 800 nm; the integrated J_{sc} is estimated to be 14.40 mA cm^{-2}, in good agreement with the *J–V* results. The low IPCE values in the red light region (from 550 nm to 800 nm) should be attributed to the poor crystalline perovskite layer (see Figure 2 C), would lead to weak light absorption in this wavelength region.[1,25,28] The solar cells prepared with the $C+CH_3NH_3I$ ink exhibit similar values at less than 550 nm to those with the C ink, but significantly higher values in the red light region. The integrated J_{sc} is estimated to be 16.80 mA cm^{-2}, which is also consistent with the *J–V* results. The improvement of IPCE in the red region should be ascribed to the high quality crystalline perovskite layer obtained with the $C+CH_3NH_3I$ ink (see Figure 2 D), which could improve charge transport and light scattering.[1,38] Besides, the improvement of the interconnectivity at the $C/CH_3NH_3PbI_3$ interface could also promote the photocurrent owing to the enhanced charge transfer and suppressed charge recombination. Figure 3 E shows the PCE distributions of the two sets of photovoltaic devices. Statistically, the overwhelming conclusion can be made that the $C+CH_3NH_3I$ ink devices (average: 10.03 %) considerably outperform the C ink devices (average: 7.55 %). Finally, long-term stability testing has been performed on the $C+CH_3NH_3I$ ink devices and the result is presented in Figure 3 F. Significantly, the $C+CH_3NH_3I$ ink device retained about 90 % of the highest PCE (measured one day after the device was fabricated) even after storage for 12 days. Therefore, the obtained nanocarbon-based perovskite solar cells appear to be significantly more stable[29] than the conventional spiro-OMeTAD-based cells, for which the environmental instability, especially in humid air, has been widely recognized.[11,17]

To gain a deeper insight into the improvement in V_{oc} and FF by $C+CH_3NH_3I$ ink, we resorted to electrochemical impedance spectroscopy (EIS), which is a powerful technique for investigating charge transfer behaviors at the interfaces in solar cells. The complex plane impedance plots for the two solar cells at different forward applied biases (V_{appl}) (0.2 V and 0.8 V) are presented in Figure 4 A and B. Two obvious semicircles are observed for both solar cells at a certain V_{appl}, corresponding to two significantly different charge-transfer or transport behaviors. As reported previously, two such semicircles were also detected in perovskite solar cells containing organic HTM,[40,41] and ascribed to the charge transport in HTM at high frequencies and to the charge transfer at the $CH_3NH_3PbI_3$/HTM interface at low frequencies. In our case, therefore, the high-frequency semicircle may be related to the charge transport in the C counter electrode, while the lower-frequency semicircle may reflect the charge transfer at the $CH_3NH_3PbI_3$/C interface. Clearly, the diameter of the low-frequency semicircle strongly depends on V_{appl}, that is, the higher the V_{appl}, the smaller the semicircle diameter, testifying the attribution of the low-frequency semicircle to charge transfer at the $CH_3NH_3PbI_3$/C interface. This is because the increase of V_{appl} upshifts the Fermi level of $CH_3NH_3PbI_3$, promotes the electron transfer from $CH_3NH_3PbI_3$ to C (recombination reaction) and hence lowers the recombination resistance (R_{rec}).[40]

To further understand charge transfer properties of the $CH_3NH_3PbI_3$/C interface, R_{rec} was obtained by fitting the complex plane impedance plots at different V_{appl} using the

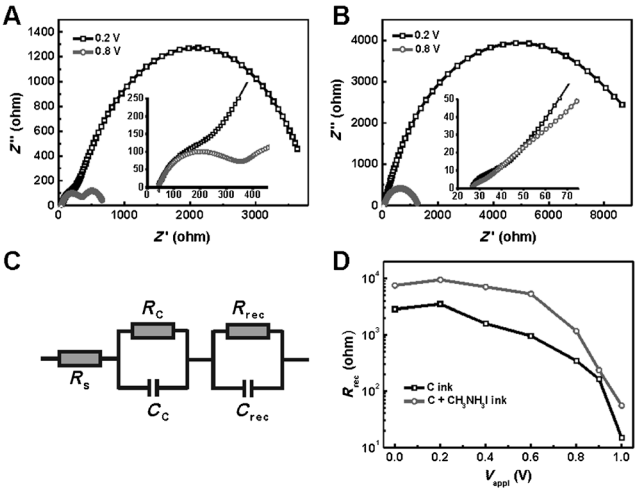

Figure 4. Impedance spectroscopy characterization: A), B) Complex plane impedance plots of the $TiO_2/CH_3NH_3PbI_3$/C solar cells prepared with (A) the C ink and (B) the C + CH_3NH_3I ink at different V_{appl} (0.2 V and 0.8 V) under dark conditions. C) Equivalent circuit used for modeling, where R_s is the series resistance, R_c/C_c the resistance/capacitance associated with the carbon electrode, and R_{rec}/C_{rec} the resistance/capacitance related to the C/$CH_3NH_3PbI_3$ interface. D) Recombination resistance (R_{rec})–V_{appl} curves for both solar cells.

equivalent circuit sketched in Figure 4C. Notably, the R_{rec} for the C + CH_3NH_3I ink-based solar cell is several times higher than that prepared with the C ink in the whole V_{appl} range, indicating much more significant suppression of charge recombination at the $CH_3NH_3PbI_3$/C interface in the former cell. Such distinctive charge recombination behaviors should be an important factor in determining the different V_{oc} values observed for the two solar cells.[40,42,43]

In conclusion, we have demonstrated a successful fabrication of the first planar carbon-based perovskite solar cells for which an inkjet printing technique was developed to deposit the nanocarbon electrode. The inkjet printing technique could not only precisely and controllably pattern the carbon electrode, but also improve the interface between the $CH_3NH_3PbI_3$ and C electrodes by the instant chemical transformation. By exploiting the C + CH_3NH_3I ink formulation to transform PbI_2 in situ to $CH_3NH_3PbI_3$, a reinforced interpenetrating interface between the $CH_3NH_3PbI_3$ and C electrodes was formed in comparison with that using bare C ink, which significantly suppressed charge recombination at the interface. As a result, a considerably high PCE up to 11.60% was achieved. Therefore, our work holds promise for producing low cost, large-scale, and highly efficient perovskite solar cells using inkjet printing related techniques.

Received: August 28, 2014
Published online: September 24, 2014

Keywords: inkjet printing · nanocarbon · perovskite · solar cells

[1] Z. Xiao, C. Bi, Y. Shao, Q. Dong, Q. Wang, Y. Yuan, C. Wang, Y. Gao, J. Huang, *Energy Environ. Sci.* **2014**, *7*, 2619 – 2623.
[2] K. Wojciechowski, M. Saliba, T. Leijtens, A. Abate, H. J. Snaith, *Energy Environ. Sci.* **2014**, *7*, 1142 – 1147.
[3] Q. Wang, Y. C. Shao, Q. F. Dong, Z. G. Xiao, Y. B. Yuan, J. S. Huang, *Energy Environ. Sci.* **2014**, *7*, 2359 – 2365.
[4] N. J. Jeon, H. G. Lee, Y. C. Kim, J. Seo, J. H. Noh, J. Lee, S. I. Seok, *J. Am. Chem. Soc.* **2014**, *136*, 7837 – 7840.
[5] S. Ryu, J. H. Noh, N. J. Jeon, Y. Chan Kim, W. S. Yang, J. Seo, S. I. Seok, *Energy Environ. Sci.* **2014**, *7*, 2614 – 2618.
[6] M. Z. Liu, M. B. Johnston, H. J. Snaith, *Nature* **2013**, *501*, 395 – 398.
[7] J. Burschka, N. Pellet, S. J. Moon, R. Humphry-Baker, P. Gao, M. K. Nazeeruddin, M. Gratzel, *Nature* **2013**, *499*, 316 – 318.
[8] H. S. Kim, C. R. Lee, J. H. Im, K. B. Lee, T. Moehl, A. Marchioro, S. J. Moon, R. Humphry-Baker, J. H. Yum, J. E. Moser, M. Gratzel, N. G. Park, *Sci. Rep.* **2012**, *2*, 591 – 598.
[9] A. Kojima, K. Teshima, Y. Shirai, T. Miyasaka, *J. Am. Chem. Soc.* **2009**, *131*, 6050 – 6051.
[10] N. J. Jeon, J. H. Noh, Y. C. Kim, W. S. Yang, S. Ryu, S. I. Seok, *Nat. Mater.* **2014**, *13*, 897 – 903.
[11] H. Zhou, Q. Chen, G. Li, S. Luo, T.-b. Song, H.-S. Duan, Z. Hong, J. You, Y. Liu, Y. Yang, *Science* **2014**, *345*, 542 – 546.
[12] C. S. Ponseca, T. J. Savenije, M. Abdellah, K. Zheng, A. Yartsev, T. Pascher, T. Harlang, P. Chabera, T. Pullerits, A. Stepanov, J.-P. Wolf, V. Sundström, *J. Am. Chem. Soc.* **2014**, *136*, 5189 – 5192.
[13] G. C. Xing, N. Mathews, S. Y. Sun, S. S. Lim, Y. M. Lam, M. Gratzel, S. Mhaisalkar, T. C. Sum, *Science* **2013**, *342*, 344 – 347.
[14] Z. Zhu, J. Ma, Z. Wang, C. Mu, Z. Fan, L. Du, Y. Bai, L. Fan, H. Yan, D. L. Phillips, S. Yang, *J. Am. Chem. Soc.* **2014**, *136*, 3760 – 3763.
[15] J. Qiu, Y. Qiu, K. Yan, M. Zhong, C. Mu, H. Yan, S. Yang, *Nanoscale* **2013**, *5*, 3245 – 3248.
[16] W. Yongzhen, A. Islam, X. Yang, C. Qin, J. Liu, K. Zhang, W. Peng, L. Han, *Energy Environ. Sci.* **2014**, *7*, 2934 – 2938.
[17] J. Liu, W. Yongzhen, C. Qin, X. Yang, T. Yasuda, A. Islam, K. Zhang, W. Peng, L. Han, W. Chen, *Energy Environ. Sci.* **2014**, *7*, 2963 – 2967.
[18] P. Qin, S. Tanaka, S. Ito, N. Tetreault, K. Manabe, H. Nishino, M. K. Nazeeruddin, M. Gratzel, *Nat. Commun.* **2014**, *5*, 3834 – 3840.
[19] J. A. Christians, R. C. Fung, P. V. Kamat, *J. Am. Chem. Soc.* **2014**, *136*, 758 – 764.
[20] S. Aharon, S. Gamliel, B. E. Cohen, L. Etgar, *Phys. Chem. Chem. Phys.* **2014**, *16*, 10512 – 10518.
[21] W. A. Laban, L. Etgar, *Energy Environ. Sci.* **2013**, *6*, 3249 – 3253.
[22] Y. Xu, J. Shi, S. Lv, L. Zhu, J. Dong, H. Wu, Y. Xiao, Y. Luo, S. Wang, D. Li, X. Li, Q. Meng, *ACS Appl. Mater. Interfaces* **2014**, *6*, 5651 – 5656.
[23] J. J. Shi, J. Dong, S. T. Lv, Y. Z. Xu, L. F. Zhu, J. Y. Xiao, X. Xu, H. J. Wu, D. M. Li, Y. H. Luo, Q. B. Meng, *Appl. Phys. Lett.* **2014**, *104*, 063901 – 063905.
[24] J. Shi, Y. Luo, H. Wei, J. Luo, J. Dong, S. Lv, J. Xiao, Y. Xu, L. Zhu, X. Xu, H. Wu, D. Li, Q. Meng, *ACS Appl. Mater. Interfaces* **2014**, *6*, 9711 – 9718.
[25] Y. Rong, Z. Ku, A. Mei, T. Liu, M. Xu, S. Ko, X. Li, H. Han, *J. Phys. Chem. Lett.* **2014**, *5*, 2160 – 2164.
[26] Z. Li, S. A. Kulkarni, P. P. Boix, E. Shi, A. Cao, K. Fu, S. K. Batabyal, J. Zhang, Q. Xiong, L. H. Wong, N. Mathews, S. G. Mhaisalkar, *ACS Nano* **2014**, *8*, 6797 – 6804.
[27] H. Han, M. Xu, Y. Rong, Z. Ku, A. Mei, T. Liu, L. Zhang, *J. Mater. Chem. A* **2014**, *2*, 8607 – 8611.
[28] Z. Ku, Y. Rong, M. Xu, T. Liu, H. Han, *Sci. Rep.* **2013**, *3*, 3132 – 3137.
[29] A. Mei, X. Li, L. Liu, Z. Ku, T. Liu, Y. Rong, M. Xu, M. Hu, J. Chen, Y. Yang, M. Grätzel, H. Han, *Science* **2014**, *345*, 295 – 298.
[30] Z. Wei, K. Yan, H. Chen, Y. Yi, T. Zhang, X. Long, J. Li, L. Zhang, J. Wang, S. Yang, *Energy Environ. Sci.* **2014**, *7*, 3326 – 3333.

[31] M. He, D. Zheng, M. Wang, C. Lin, Z. Lin, *J. Mater. Chem. A* **2014**, *2*, 5994 – 6003.
[32] G. E. Eperon, S. D. Stranks, C. Menelaou, M. B. Johnston, L. Herz, H. Snaith, *Energy Environ. Sci.* **2014**, *7*, 982 – 988.
[33] G. E. Eperon, V. M. Burlakov, P. Docampo, A. Goriely, H. J. Snaith, *Adv. Funct. Mater.* **2014**, *24*, 151 – 157.
[34] P. Docampo, F. Hanusch, S. D. Stranks, M. Döblinger, J. M. Feckl, M. Ehrensperger, N. K. Minar, M. B. Johnston, H. J. Snaith, T. Bein, *Adv. Energy Mater.* **2014**, DOI: 10.1002/aenm.201400355.
[35] J. Y. Jeng, Y. F. Chiang, M. H. Lee, S. R. Peng, T. F. Guo, P. Chen, T. C. Wen, *Adv. Mater.* **2013**, *25*, 3727 – 3732.
[36] P. Docampo, J. M. Ball, M. Darwich, G. E. Eperon, H. J. Snaith, *Nat. Commun.* **2013**, *4*, 2761 – 2767.
[37] Q. Chen, H. Zhou, Z. Hong, S. Luo, H.-S. Duan, H.-H. Wang, Y. Liu, G. Li, Y. Yang, *J. Am. Chem. Soc.* **2014**, *136*, 622 – 625.
[38] A. Yella, L.-P. Heiniger, P. Gao, M. K. Nazeeruddin, M. Grätzel, *Nano Lett.* **2014**, *14*, 2591 – 2596.
[39] J. You, Z. Hong, Y. Yang, Q. Chen, M. Cai, T.-B. Song, C.-C. Chen, S. Lu, Y. Liu, H. Zhou, Y. Yang, *ACS Nano* **2014**, *8*, 1674 – 1680.
[40] V. Gonzalez-Pedro, E. J. Juarez-Perez, W. S. Arsyad, E. M. Barea, F. Fabregat-Santiago, I. Mora-Sero, J. Bisquert, *Nano Lett.* **2014**, *14*, 888 – 893.
[41] A. Dualeh, T. Moehl, N. Tétreault, J. Teuscher, P. Gao, M. K. Nazeeruddin, M. Grätzel, *ACS Nano* **2014**, *8*, 362 – 373.
[42] F. Fabregat-Santiago, G. Garcia-Belmonte, I. Mora-Sero, J. Bisquert, *Phys. Chem. Chem. Phys.* **2011**, *13*, 9083 – 9118.
[43] R. S. Sanchez, V. Gonzalez-Pedro, J.-W. Lee, N.-G. Park, Y. S. Kang, I. Mora-Sero, J. Bisquert, *J. Phys. Chem. Lett.* **2014**, *5*, 2357 – 2363.

